Applied Numerical Mathematics 165 (2021) 482–499

Contents lists available at ScienceDirect

Applied Numerical Mathematics

www.elsevier.com/locate/apnum

High-order Runge-Kutta discontinuous Galerkin methods with multi-resolution WENO limiters for solving steady-state problems

Jun Zhu [a,1], Chi-Wang Shu [b,2], Jianxian Qiu [c,*,3]

[a] College of Science, Nanjing University of Aeronautics and Astronautics, Nanjing, Jiangsu 210016, PR China
[b] Division of Applied Mathematics, Brown University, Providence, RI 02912, USA
[c] School of Mathematical Sciences and Fujian Provincial Key Laboratory of Mathematical Modeling and High-Performance Scientific Computing, Xiamen University, Xiamen, Fujian 361005, PR China

ARTICLE INFO

Article history:
Received 19 September 2020
Received in revised form 20 January 2021
Accepted 12 March 2021
Available online 18 March 2021

Keywords:
Multi-resolution WENO limiter
RKDG method
Slight post-shock oscillation
Machine zero
Steady-state problem

ABSTRACT

Since the classical WENO schemes [27] might suffer from slight post-shock oscillations (which are responsible for the numerical residual to hang at a truncation error level) and the new high-order multi-resolution WENO schemes [59] are successful to solve for steady-state problems, we apply these high-order finite volume multi-resolution WENO techniques to serve as limiters for high-order Runge-Kutta discontinuous Galerkin (RKDG) methods in simulating steady-state problems. Firstly, a new troubled cell indicator is designed to precisely detect the cells which would need further limiting procedures. Then the high-order multi-resolution WENO limiting procedures are adopted on a sequence of hierarchical L^2 projection polynomials of the DG solution within the troubled cell itself. By doing so, these RKDG methods with multi-resolution WENO limiters could gradually degrade from the optimal high-order accuracy to the first-order accuracy near strong discontinuities, suppress the slight post-shock oscillations, and push the numerical residual to settle down to machine zero in steady-state simulations. These new multi-resolution WENO limiters are very simple to construct and can be easily implemented to arbitrary high-order accuracy for solving steady-state problems in multi-dimensions.

1. Introduction

In this paper, high-order Runge-Kutta discontinuous Galerkin (RKDG) methods [8–10,12] with new multi-resolution WENO limiters [58] are applied to solve steady Euler equations

$$\begin{cases} f(u)_x + g(u)_y = 0, \\ u(x, y) = u_0(x, y), \end{cases} \tag{1.1}$$

* Corresponding author.
E-mail addresses: zhujun@nuaa.edu.cn (J. Zhu), chi-wang_shu@brown.edu (C.-W. Shu), jxqiu@xmu.edu.cn (J. Qiu).

[1] Research was supported by NSFC grant 11872210 and Science Challenge Project, No. TZ2016002. The author was also partly supported by NSFC grant 11926103 when he visited Tianyuan Mathematical Center in Southeast China, Xiamen, Fujian 361005, P.R. China.
[2] Research was supported by AFOSR grant FA9550-20-1-0055 and NSF grant DMS-2010107.
[3] Research was supported by NSFC grant 12071392 and Science Challenge Project, No. TZ2016002.

https://doi.org/10.1016/j.apnum.2021.03.011
0168-9274/

on structured meshes. One way to get a numerical solution of (1.1) is to solve the associated unsteady Euler equations

$$\begin{cases} u_t + f(u)_x + g(u)_y = 0, \\ u(x, y, 0) = u_0(x, y), \end{cases} \tag{1.2}$$

and then drive the numerical residual to zero. High-order DG methods are applied to discretize the spatial variables and explicit, nonlinearly stable high-order Runge-Kutta methods [47,13] are adopted to discretize the temporal variable. Our main objective of this paper is to design a new troubled cell indicator to precisely detect the cells that need further limiting procedures and then adopt the arbitrary high-order spatial limiting procedures [58] for the RKDG methods to solve two-dimensional steady-state problems.

If one confirms that the numerical residual of the unsteady Euler equations (1.2) is small enough, ideally at or close to the level of machine zero, the numerical solution of the steady Euler equations (1.1) is acceptable. The appearance of strong discontinuities in the simulation of (1.1) and (1.2) is the main difficulty. If the numerical solution has strong shocks or contact discontinuities, its physical variables change abruptly. Many high-resolution numerical schemes have been designed with the aim of controlling the oscillations by the use of artificial viscosities [24,25] or limiters [20,24,50]. Jameson et al. [23,26] proposed a third-order finite volume discretization method with dissipative terms and applied a Runge-Kutta time discretization method for solving the steady Euler equations. However, the main drawback of such schemes is that one often needs to adjust certain parameters in the artificial viscosity to maintain sharp shock transitions and to suppress oscillations near strong shocks. If limiters are used in designing numerical schemes, such numerical schemes could be very efficient in computing supersonic flows including strong shocks and contact discontinuities [20]. Yet the application of total variation diminishing (TVD) type limiters will degrade the accuracy of the numerical scheme to first-order near local smooth extrema [41], and the lack of sufficient smoothness of the numerical fluxes with the application of such limiters often results in the numerical residual not converging close to machine zero. Yee et al. [53] designed an implicit stable high-resolution TVD scheme and applied it to compute steady-state problems. Yee and Harten [52] designed TVD schemes to solve multi-dimensional hyperbolic conservation laws and steady-state problems in curvilinear coordinates. In 1996, Jiang and Shu [27] designed a fifth-order finite difference WENO scheme. When the classical high-order WENO schemes [27] are used to solve for the steady-state problems, their numerical residual often hangs at a truncation error level without settling down close to machine zero even after a long time iteration. Serna et al. [45] proposed a new limiter to reconstruct the numerical flux and improve the convergence of the numerical solution to steady states. Zhang et al. [57] found that slight post-shock oscillations would propagate from the region near the shocks downstream to the smooth regions and result in the numerical residual hanging at a high truncation error level rather than converging to machine zero. Zhang et al. [54] designed an upwind-biased interpolation technique to improve the convergence of high-order WENO scheme for steady-state problems. But the numerical residual computed by such new schemes still could not converge close to machine zero for some two-dimensional steady-state problems [54]. In 2016, a novel high-order fixed-point sweeping WENO method [51] was proposed to simulate steady-state problems and could obtain better convergence property. However, the numerical residual could not settle down close to machine zero for some benchmark steady-state tests as before.

Now let us first review the history of the development of discontinuous Galerkin (DG) methods. In 1973, Reed and Hill [44] designed the first DG method in the framework of neutron transport. Due to its desirable properties, DG methods were also used extensively in different fields [14,21,29,33,40]. The hybrid DG/FV methods [15,16,36,55,56] which combine the advantageous features of both have become popular. Luo et al. [36,38] designed a new DG method for solving the compressible equations with a Taylor basis. If unsteady or steady-state problems are not smooth enough, their numerical solutions might contain oscillations near strong discontinuities and result in nonlinear instability in nonsmooth regions. One possible methodology to suppress oscillations is to apply nonlinear limiters to the high-order RKDG methods. A major development of the DG method with a classical *minmod* type total variation bounded (TVB) limiter was carried out by Cockburn et al. in a series of papers [8–12]. One type of limiters is based on slope modification, such as classical *minmod* type limiters [8–10,12], the Barth-Jespersen limiter [2], the Venkatakrishnan limiter [50], the moment based limiter [3], and an improved moment limiter [5]. Such limiters belong to the slope type limiters and they could suppress oscillations at the price of possibly degrading numerical accuracy at smooth extrema. Another type of limiters is based on the essentially non-oscillatory (ENO), weighted ENO (WENO), and Hermite WENO (HWENO) methodologies [1,17,18,22,27,32,34,35,37,39], which can achieve uniform high-order accuracy in smooth regions and keep essentially non-oscillatory property near strong discontinuities. However, it is very difficult to implement RKDG methods with the applications of WENO limiters for solving steady-state problems. When such high-order RKDG methods are applied to compute steady Euler equations, the numerical residual could not converge close to machine zero and would hang at a higher truncation error level.

Likewise, when the classical fifth-order finite difference WENO scheme [27,46] with a third-order TVD Runge-Kutta time discretization [47] is used to solve for the steady-state problems, the numerical residual often hangs at the truncation error level instead of converging to machine zero even after a long time iteration. Yet the numerical residual of the new high-order finite difference and finite volume multi-resolution WENO schemes [60] could converge close to machine zero without introducing any slight post-shock oscillations on structured meshes. With the application of a series of unequal-sized spatial stencils, the multi-resolution WENO schemes could gradually degrade from the optimal high-order accuracy to the first-order accuracy near strong discontinuities. We think this is the most important reason that the numerical residual of the classical fifth-order finite difference WENO scheme [27,46] could not convergence to a tiny number, since its spatial approximation could not degrade to the first-order accuracy with the application of equal-sized three-point spatial stencils.

Table 1
2D Euler equations. Case (1). RKDG methods with multi-resolution WENO limiters. Steady state. L^1 and L^∞ errors.

	Second-order method				Third-order method			
Grid cells	L^1 error	Order	L^∞ error	Order	L^1 error	Order	L^∞ error	Order
20×20	9.04E-5		9.42E-4		3.43E-6		2.29E-5	
30×30	4.01E-5	2.00	4.22E-4	1.98	1.02E-6	2.98	7.00E-6	2.92
40×40	2.25E-5	2.00	2.38E-4	1.99	4.33E-7	2.99	2.98E-6	2.96
50×50	1.44E-5	2.00	1.52E-4	1.99	2.22E-7	2.99	1.53E-6	2.98
60×60	1.00E-5	2.00	1.06E-4	1.99	1.28E-7	2.99	8.91E-7	2.99
	Fourth-order method				Fifth-order method			
Grid cells	L^1 error	Order	L^∞ error	Order	L^1 error	Order	L^∞ error	Order
20×20	2.46E-8		2.59E-7		4.29E-10		3.08E-9	
30×30	4.81E-9	4.03	5.12E-8	4.00	5.58E-11	5.03	4.10E-10	4.97
40×40	1.51E-9	4.02	1.62E-8	4.00	1.31E-11	5.02	9.77E-11	4.98
50×50	6.17E-10	4.02	6.64E-9	4.00	4.31E-12	5.01	3.21E-11	4.98
60×60	2.96E-10	4.01	3.20E-9	4.00	1.74E-12	4.97	1.29E-11	4.97

Table 2
2D Euler equations. Case (2). RKDG methods with multi-resolution WENO limiters. Steady state. L^1 and L^∞ errors.

	Second-order method				Third-order method			
Grid cells	L^1 error	Order	L^∞ error	Order	L^1 error	Order	L^∞ error	Order
20×20	4.60E-4		3.62E-3		2.43E-5		1.82E-4	
30×30	1.91E-4	2.17	1.61E-3	1.99	7.32E-6	2.96	5.54E-5	2.94
40×40	1.04E-4	2.09	9.10E-4	2.00	3.11E-6	2.98	2.36E-5	2.96
50×50	6.61E-5	2.05	5.83E-4	2.00	1.59E-6	2.98	1.21E-5	2.98
60×60	4.56E-5	2.03	4.05E-4	2.00	9.27E-7	2.99	7.04E-6	2.99
	Fourth-order method				Fifth-order method			
Grid cells	L^1 error	Order	L^∞ error	Order	L^1 error	Order	L^∞ error	Order
20×20	4.51E-7		4.14E-6		1.27E-8		9.31E-8	
30×30	8.77E-8	4.04	8.18E-7	4.00	1.64E-9	5.06	1.27E-8	4.90
40×40	2.75E-8	4.03	2.59E-7	4.00	3.85E-10	5.04	3.08E-9	4.95
50×50	1.12E-8	4.02	1.06E-7	4.00	1.25E-10	5.03	1.01E-9	4.97
60×60	5.40E-9	4.01	5.12E-8	4.00	5.02E-11	5.02	4.10E-10	4.98

So we extend high-order RKDG methods with high-order multi-resolution WENO limiters [58] to solve for the steady Euler equations with the application of a new troubled cell indicator on structured meshes. This new troubled cell indicator is very simple and works well for precisely detecting the cells that need further limiting procedure. To the best of our knowledge, it is the first type of high-order RKDG methods with WENO limiters that could confirm the numerical residual to converge close to machine zero for two-dimensional steady-state problems containing strong shocks at the boundary.

This paper is organized as follows. In Section 2, we give a brief review of the RKDG methods. In Section 3, we propose a new troubled cell indicator to detect the cells needing further limiting procedures and design arbitrary high-order limiting procedures using second-order, third-order, fourth-order, and fifth-order multi-resolution WENO limiters for steady-state computations as examples. In Section 4, several standard steady-state problems including sophisticated wave structures, both inside the computational fields and passing through the boundaries of the computational domain, are presented to demonstrate the good performance of the numerical residual converging close to machine zero. Concluding remarks are given in Section 5.

2. A brief review of the RKDG method

In this section, we first give a brief review of the RKDG methods for solving (1.2). The two-dimensional computational domain is divided by rectangular cells $I_{i,j} = I_i \times J_j = [x_{i-\frac{1}{2}}, x_{i+\frac{1}{2}}] \times [y_{j-\frac{1}{2}}, y_{j+\frac{1}{2}}]$, $i = 1, \cdots, N_x$ and $j = 1, \cdots, N_y$ with the cell sizes $x_{i+\frac{1}{2}} - x_{i-\frac{1}{2}} = \Delta x_i$, $y_{j+\frac{1}{2}} - y_{j-\frac{1}{2}} = \Delta y_j$, and cell centers $(x_i, y_j) = (\frac{1}{2}(x_{i+\frac{1}{2}} + x_{i-\frac{1}{2}}), \frac{1}{2}(y_{j+\frac{1}{2}} + y_{j-\frac{1}{2}}))$. For example, we apply the local orthonormal basis over $I_{i,j}$, $W_h^k = \{v_l^{(i,j)}(x, y),\ l = 0, ..., K;\ K = \frac{(k+1)(k+2)}{2} - 1\}$ (as shown in [58]):

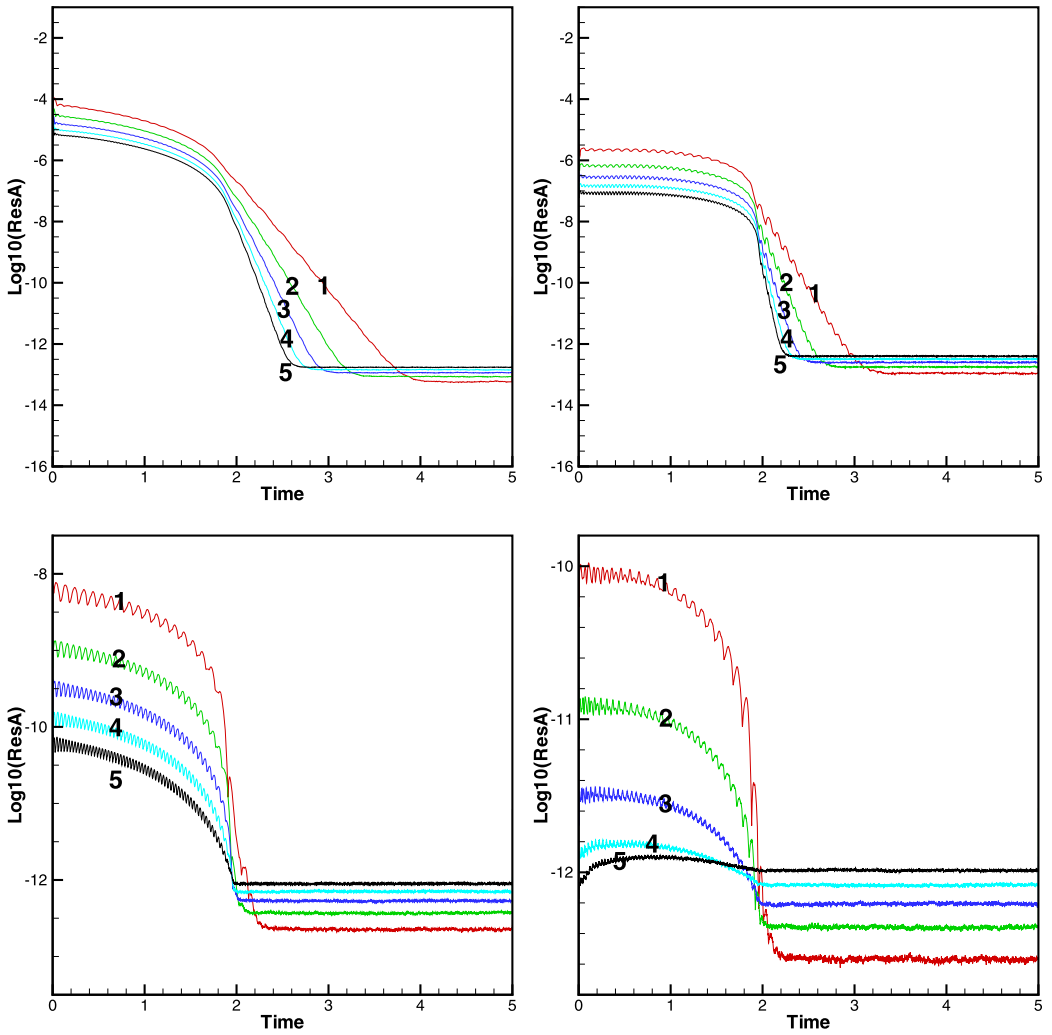

Fig. 1. 2D Euler equations. Case (1). The evolution of the average numerical residual. The results of RKDG methods with multi-resolution WENO limiters. From left to right and top to bottom: second-order, third-order, fourth-order, and fifth-order methods. Different numbers indicate different mesh levels from 20×20 to 60×60 cells.

$$
\begin{aligned}
v_0^{(i,j)}(x,y) &= 1,\\
v_1^{(i,j)}(x,y) &= \sqrt{12}\left(\tfrac{x-x_i}{\Delta x_i}\right),\\
v_2^{(i,j)}(x,y) &= \sqrt{12}\left(\tfrac{y-y_j}{\Delta y_j}\right),\\
v_3^{(i,j)}(x,y) &= \sqrt{180}\left(\left(\tfrac{x-x_i}{\Delta x_i}\right)^2 - \tfrac{1}{12}\right),\\
v_4^{(i,j)}(x,y) &= \sqrt{12}\left(\tfrac{x-x_i}{\Delta x_i}\right)\sqrt{12}\left(\tfrac{y-y_j}{\Delta y_j}\right),\\
v_5^{(i,j)}(x,y) &= \sqrt{180}\left(\left(\tfrac{y-y_j}{\Delta y_j}\right)^2 - \tfrac{1}{12}\right),\\
v_6^{(i,j)}(x,y) &= \sqrt{2800}\left(\left(\tfrac{x-x_i}{\Delta x_i}\right)^3 - \tfrac{15}{100}\left(\tfrac{x-x_i}{\Delta x_i}\right)\right),\\
v_7^{(i,j)}(x,y) &= \sqrt{180}\left(\left(\tfrac{x-x_i}{\Delta x_i}\right)^2 - \tfrac{1}{12}\right)\sqrt{12}\left(\tfrac{y-y_j}{\Delta y_j}\right),\\
v_8^{(i,j)}(x,y) &= \sqrt{12}\left(\tfrac{x-x_i}{\Delta x_i}\right)\sqrt{180}\left(\left(\tfrac{y-y_j}{\Delta y_j}\right)^2 - \tfrac{1}{12}\right),\\
v_9^{(i,j)}(x,y) &= \sqrt{2800}\left(\left(\tfrac{y-y_j}{\Delta y_j}\right)^3 - \tfrac{15}{100}\left(\tfrac{y-y_j}{\Delta y_j}\right)\right),\\
&\cdots
\end{aligned}
\tag{2.1}
$$

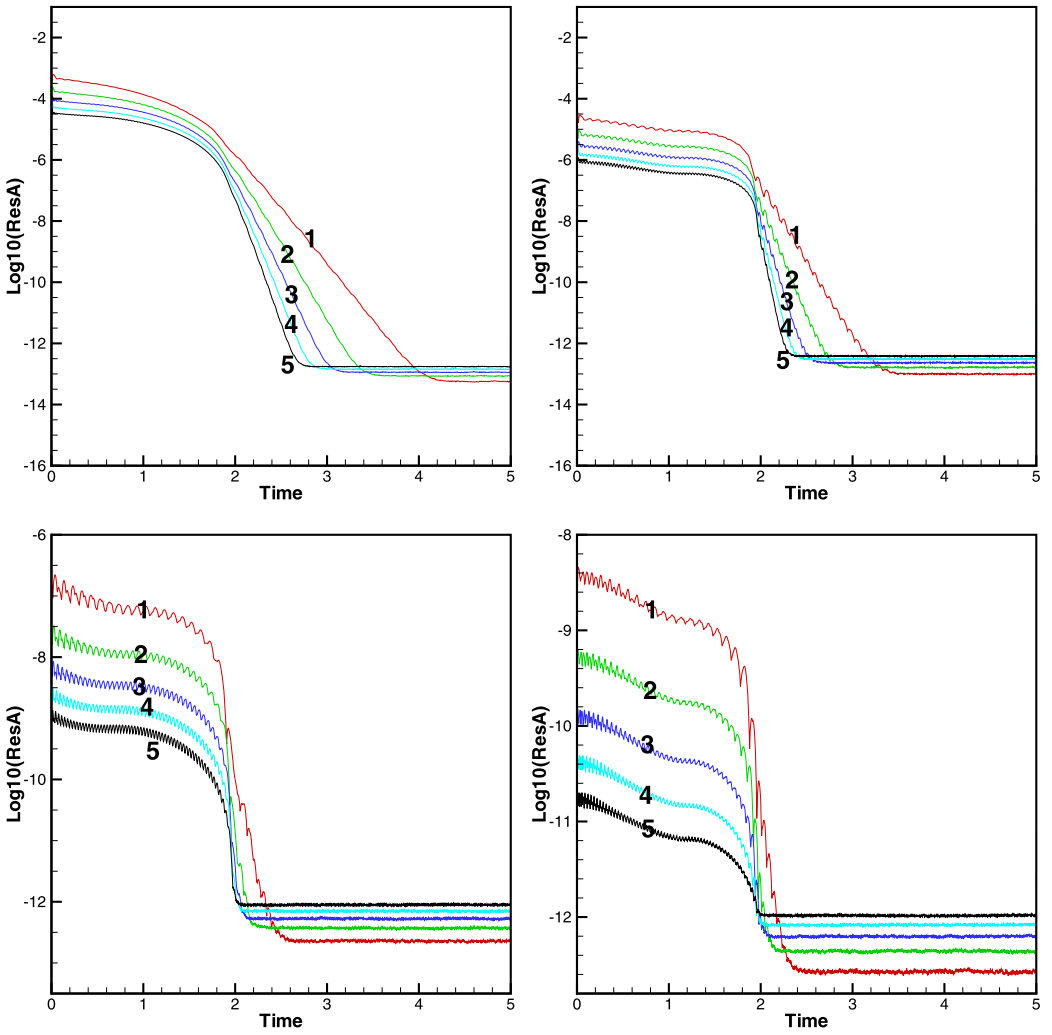

Fig. 2. 2D Euler equations. Case (2). The evolution of the average numerical residual. The results of RKDG methods with multi-resolution WENO limiters. From left to right and top to bottom: second-order, third-order, fourth-order, and fifth-order methods. Different numbers indicate different mesh levels from 20×20 to 60×60 cells.

The two-dimensional solution $u_h(x, y, t) \in W_h^k$ can be written as:

$$u_h(x, y, t) = \sum_{l=0}^{K} u_{i,j}^{(l)}(t) v_l^{(i,j)}(x, y), \quad (x, y) \in I_{i,j}, \tag{2.2}$$

and the degrees of freedom $u_{i,j}^{(l)}(t)$ are the moments defined by

$$u_{i,j}^{(l)}(t) = \frac{1}{\Delta x_i \Delta y_j} \int_{I_{i,j}} u_h(x, y, t) v_l^{(i,j)}(x, y) dxdy, \quad l = 0, ..., K. \tag{2.3}$$

In order to determine the approximation solution, we evolve the degrees of freedom $u_{i,j}^{(l)}(t)$:

$$\begin{aligned} &\frac{d}{dt} u_{i,j}^{(l)}(t) = \frac{1}{\Delta x_i \Delta y_j} \left(\int_{I_{i,j}} \left(f(u_h(x, y, t)) \frac{\partial}{\partial x} v_l^{(i,j)}(x, y) + g(u_h(x, y, t)) \frac{\partial}{\partial y} v_l^{(i,j)}(x, y) \right) dxdy \right. \\ &- \int_{I_j} \left(\hat{f}(u_h(x_{i+\frac{1}{2}}, y, t)) v_l^{(i,j)}(x_{i+\frac{1}{2}}, y) - \hat{f}(u_h(x_{i-\frac{1}{2}}, y, t)) v_l^{(i,j)}(x_{i-\frac{1}{2}}, y) \right) dy \\ &\left. - \int_{I_i} \left(\hat{g}(u_h(x, y_{j+\frac{1}{2}}, t)) v_l^{(i,j)}(x, y_{j+\frac{1}{2}}) - \hat{g}(u_h(x, y_{j-\frac{1}{2}}, t)) v_l^{(i,j)}(x, y_{j-\frac{1}{2}}) \right) dx \right), \\ &l = 0, ..., K, \end{aligned} \tag{2.4}$$

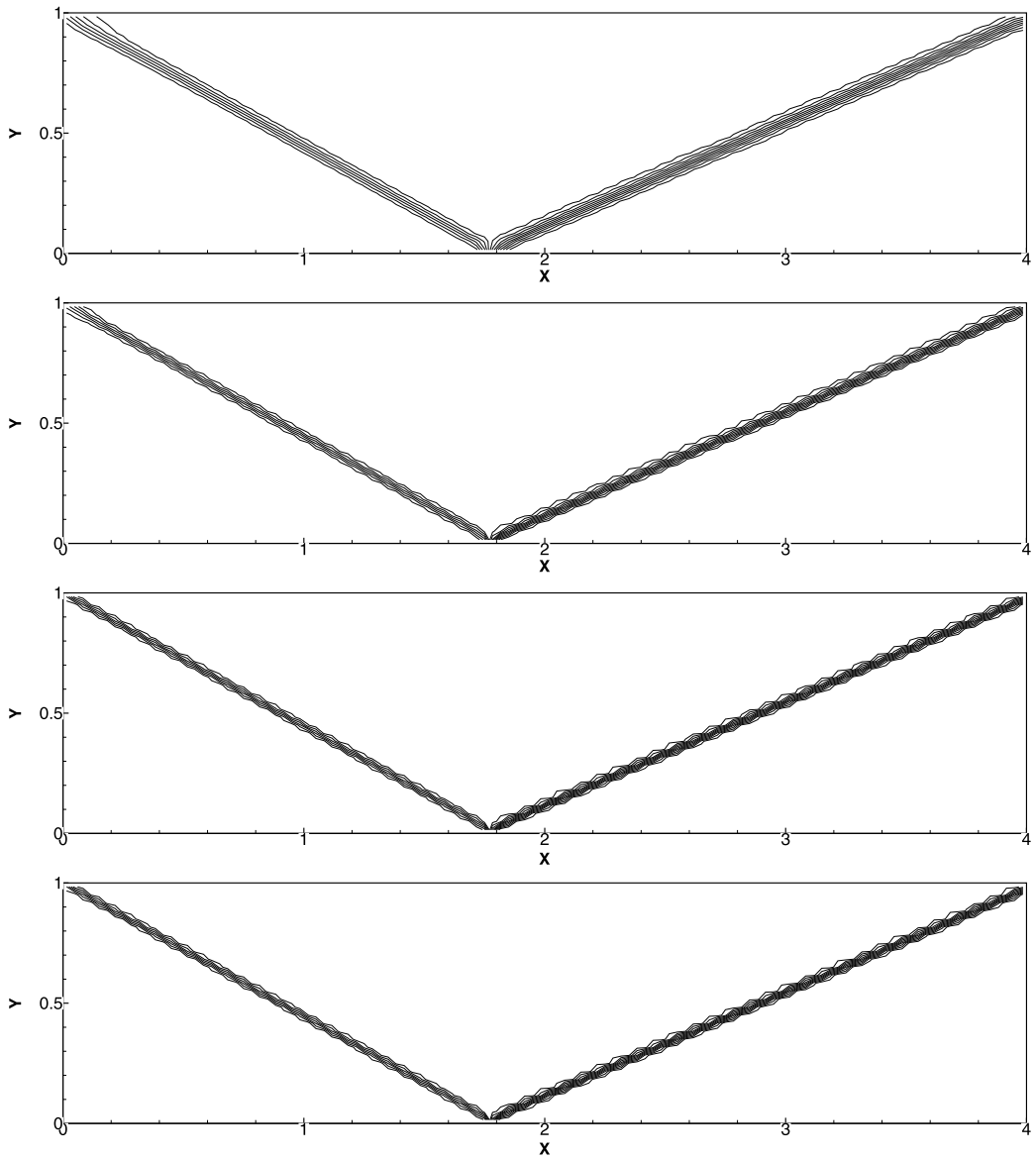

Fig. 3. The shock reflection problem. 15 equally spaced density contours from 1.10 to 2.58. The results of RKDG methods with multi-resolution WENO limiters. From top to bottom: second-order, third-order, fourth-order, and fifth-order methods. 120×30 cells.

where the "hat" terms are the numerical fluxes ($\hat{f}$ and $\hat{g}$ are monotone fluxes for the scalar case and exact or approximate Riemann solvers for the system case). The integrals in (2.4) are computed by applying suitable numerical quadratures. The semi-discrete scheme (2.4) can be discretized in time by a third-order TVD Runge-Kutta time discretization method [47]:

$$\begin{cases} u^{(1)} &= u^n + \Delta t L(u^n), \\ u^{(2)} &= \frac{3}{4}u^n + \frac{1}{4}u^{(1)} + \frac{1}{4}\Delta t L(u^{(1)}), \\ u^{n+1} &= \frac{1}{3}u^n + \frac{2}{3}u^{(2)} + \frac{2}{3}\Delta t L(u^{(2)}). \end{cases} \tag{2.5}$$

In order to explain how to apply a nonlinear limiter for the RKDG methods, we adopt a forward Euler time discretization of (2.4) as an example. Starting from a solution $u_h^n \in W_h^k$ at time level n, we limit it to obtain a new function $u^{n,new}$ before advancing it to the next time level. We need to find $u_h^{n+1} \in W_h^k$ which satisfies

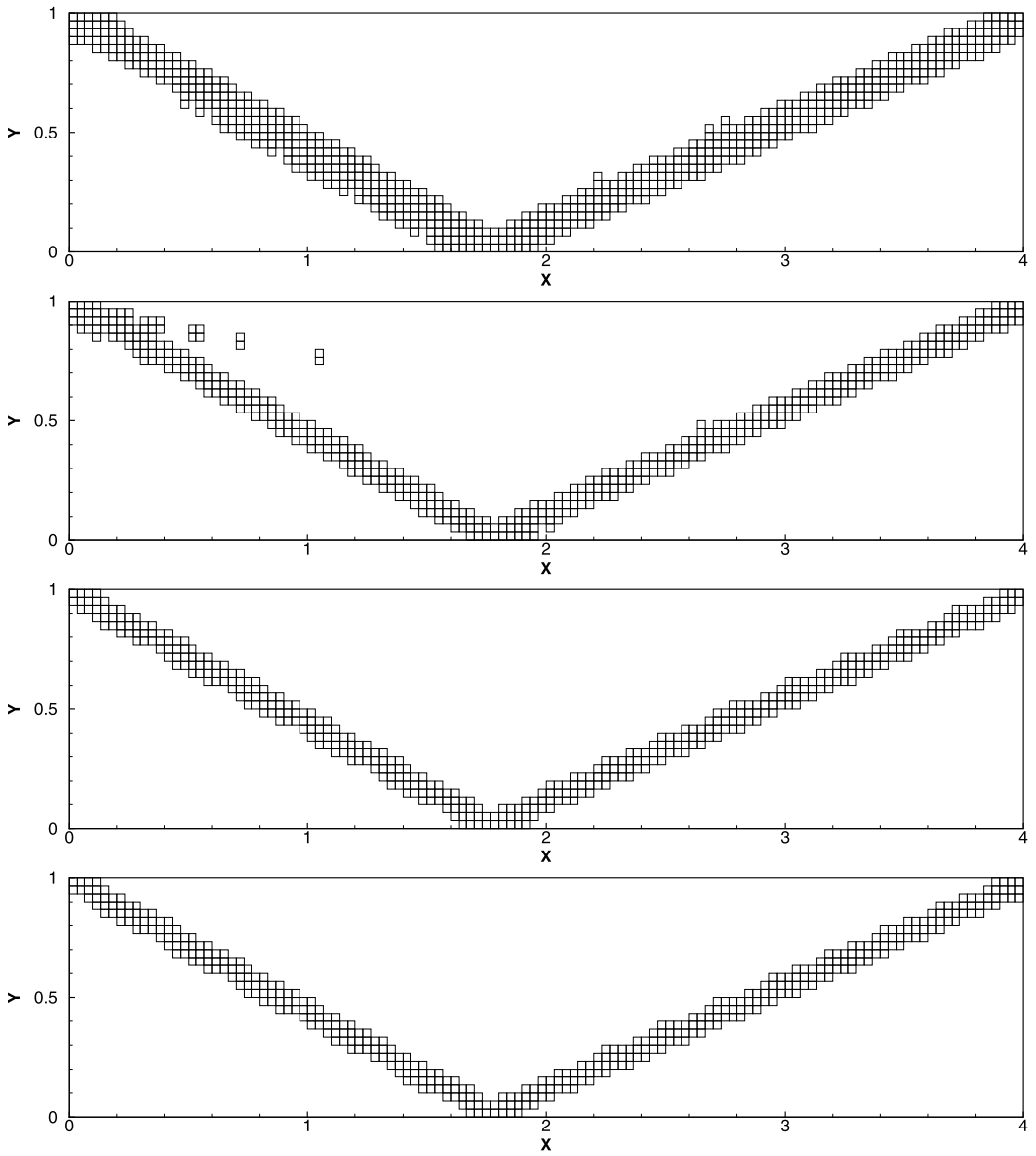

Fig. 4. The shock reflection problem. Troubled cells. Squares denote cells which are identified as troubled cells subject to multi-resolution WENO limiting procedures at the last time step. From top to bottom: second-order, third-order, fourth-order, and fifth-order methods. 120×30 cells.

$$
\begin{aligned}
&\int_{I_{i,j}} \frac{u_h^{n+1}-u_h^{n,new}}{\Delta t} v\, dxdy - \int_{I_{i,j}} \left(f(u_h^{n,new}) v_x + g(u_h^{n,new}) v_y \right) dxdy \\
&+ \int_{I_j} \left(\hat{f}(u_h^{n,new}|_{x=x_{i+\frac{1}{2}}}) v(x_{i+\frac{1}{2}}^-, y) - \hat{f}(u_h^{n,new}|_{x=x_{i-\frac{1}{2}}}) v(x_{i-\frac{1}{2}}^+, y) \right) dy \\
&+ \int_{I_i} \left(\hat{g}(u_h^{n,new}|_{y=y_{j+\frac{1}{2}}}) v(x, y_{j+\frac{1}{2}}^-) - \hat{g}(u_h^{n,new}|_{y=y_{j-\frac{1}{2}}}) v(x, y_{j-\frac{1}{2}}^+) \right) dx = 0,
\end{aligned}
\tag{2.6}
$$

for any test functions $v(x, y)$ that defined in W_h^k. We will narrate how to obtain the two-dimensional $u_h^{n,new}|_{I_{i,j}}$ in details. For simplicity, we omit the sup-indices in $u_h^{n,new}|_{I_{i,j}}$, if it does not cause confusion in the following.

3. A new troubled cell indicator and multi-resolution WENO limiter

First of all, we design a new troubled cell indicator to detect the cells that may contain strong discontinuities and in which the multi-resolution WENO limiter is applied. Other trouble cell detectors can of course also be used for solving unsteady problems, but many of them do not work well in solving steady-state problems, according to our ex-

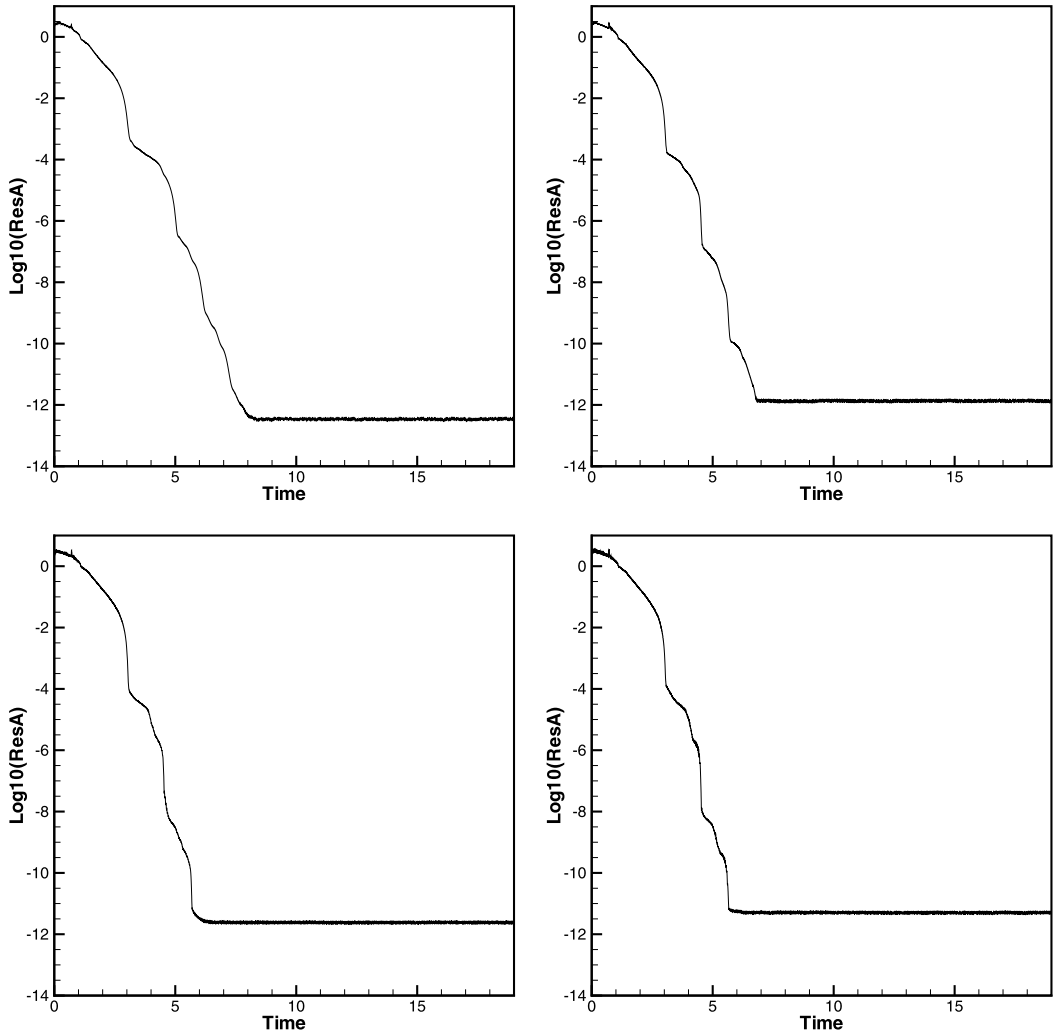

Fig. 5. The shock reflection problem. The evolution of the average numerical residual of RKDG methods with multi-resolution WENO limiters. From left to right and top to bottom: second-order, third-order, fourth-order, and fifth-order methods. 120×30 cells.

periments. With the application of (2.2), we could define $u_h|_{I_{i,j}} = u_h(x, y, t)$, for $(x, y) \in I_{i,j}$ and obtain $u_h|_{I_{i,j}} = u^{(0)}_{i,j}(t) + \sum_{l=1}^{K} u^{(l)}_{i,j}(t) v^{(i,j)}_l(x, y)$, where $u^{(0)}_{i,j}(t) = \frac{1}{\Delta x_i \Delta y_j} \int_{I_{i,j}} u_h|_{I_{i,j}} dxdy$ and similar formulas of $u_h|_{I_\ell}$ defined in other intermediate neighboring four cells of $I_{i,j}$. In two-dimensional steady-state cases, we define the cell $I_{i,j}$ to be a troubled cell when

$$\frac{\max_{I_\ell \in \{I_{i\pm1,j}, I_{i,j\pm1}\}} \left(\left| \int_{I_\ell} u_h|_{I_\ell} dxdy - \int_{I_{i,j}} u_h|_{I_{i,j}} dxdy \right| \right)}{h_{i,j} \cdot \min_{I_\ell \in \{I_{i\pm1,j}, I_{i,j\pm1}, I_{i,j}\}} \left(\left| \int_{I_\ell} u_h|_{I_\ell} dxdy \right| \right)} \geq C_k, \tag{3.1}$$

where $h_{i,j}$ is the radius of the circumscribed circle in cell $I_{i,j}$ and C_k is a constant, usually, we take $C_k = 1$ as specified in [28]. We can confirm the fact that

$$\left| \int_{I_\ell} u_h|_{I_\ell} dxdy - \int_{I_{i,j}} u_h|_{I_{i,j}} dxdy \right| = \begin{cases} O(h^3_{i,j}), & \text{in smooth regions,} \\ O(1), & \text{near a discontinuity.} \end{cases} \tag{3.2}$$

Hence the left hand side term of (3.1) converges to zero as $h_{i,j}$ converges to zero in smooth regions, whereas it converges to infinity near a discontinuity. By using (3.1), we do not need to adopt different values of C_k to compute multi-dimensional problems as in [19] and set $C_k = 1$ for the computation of all the benchmark steady-state problems. This new troubled cell indicator is simple and robust enough in simulating steady-state problems without identifying excessive troubled cells inside the computational field. We emphasize the fact that many other troubled cell indicators [8–12,28,42,43,58] are not

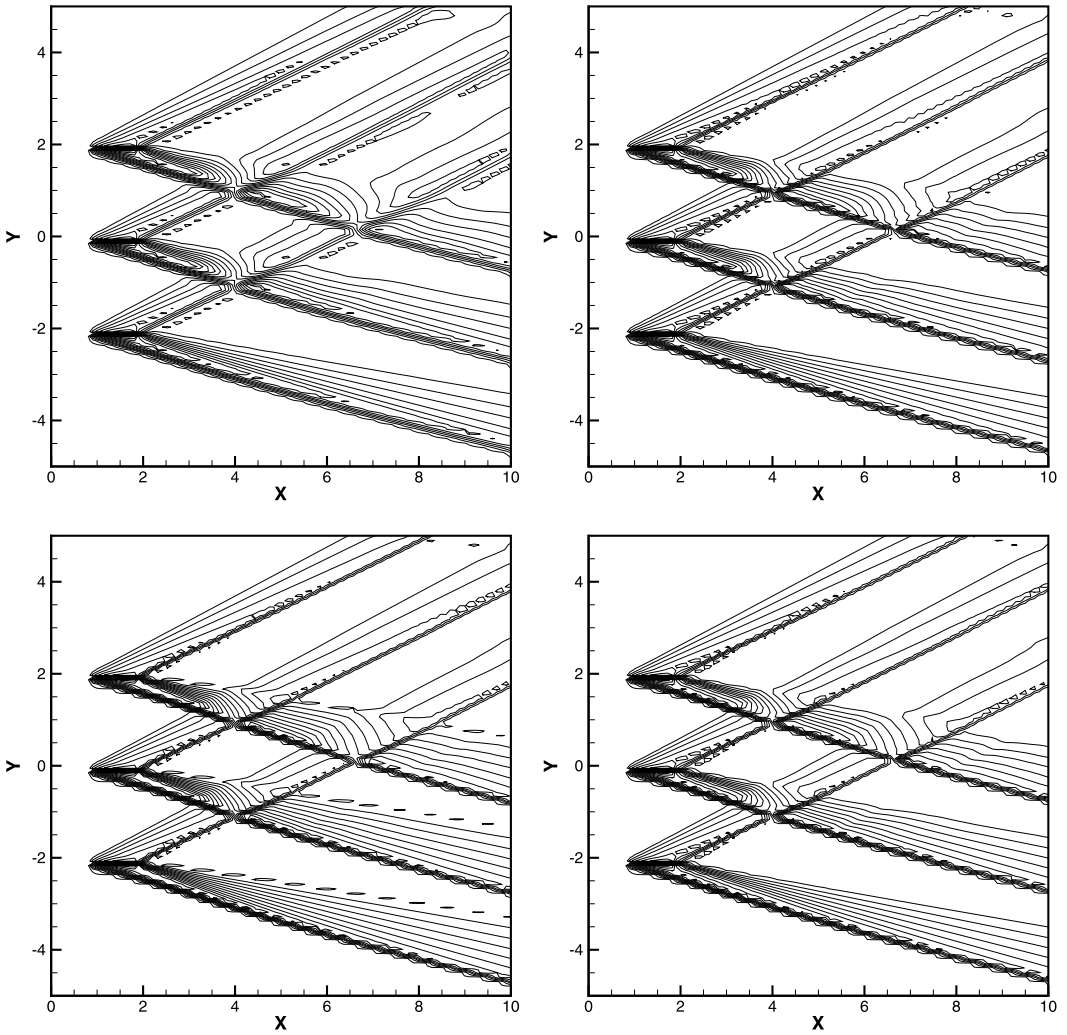

Fig. 6. A supersonic flow past three plates with an attack angle. 30 equally spaced pressure contours from 0.02 to 0.24 of RKDG methods with multi-resolution WENO limiters. From left to right and top to bottom: second-order, third-order, fourth-order, and fifth-order methods. 100×100 cells.

good at precisely detecting troubled cells for solving steady-state problems and result in the numerical residual to hang at a truncation error level instead of converging close to machine zero.

Hereafter, we give details of the multi-resolution WENO limiter for the two-dimensional scalar case. The crucial ingredient is to reconstruct a new polynomial on the troubled cell $I_{i,j}$ which is a convex combination of polynomials of different degrees: the DG solution polynomial on this cell and a sequence of hierarchical "modified" solution polynomials based on the L^2 projection methodology. For simplicity, we also rewrite $u_h(x, y, t)$ to be $u_h(x, y) \in W_h^k$ in the following, if it does not cause confusion. A series of unequal degree polynomials $q_\ell(x, y), \ell = 0, ..., k$ are constructed on the troubled cell $I_{i,j}$:

$$\int_{I_{i,j}} q_\ell(x, y) v_l^{(i,j)}(x, y) dxdy = \int_{I_{i,j}} u_h(x, y) v_l^{(i,j)}(x, y) dxdy, \ l = 0, ..., \frac{(\ell+1)(\ell+2)}{2} - 1. \tag{3.3}$$

Based on the application of the local orthonormal basis over $I_{i,j}$, the reconstructed polynomials $q_\ell(x, y), \ell = 0, ..., k$ are very simple. Since the two-dimensional solution is written in (2.2), we can directly obtain $q_\ell(x, y) = \sum_{l=0}^{\frac{(\ell+1)(\ell+2)}{2}-1} u_{i,j}^{(l)}(t) v_l^{(i,j)}(x, y)$, $\ell = 0, ..., k$, respectively. Then we obtain equivalent expressions for these constructed polynomials of different degrees. To keep consistent notation, we will denote $p_{0,1}(x, y) = q_0(x, y)$. Following the original ideas for classical CWENO schemes [6,30,31], we obtain polynomials $p_{\ell,\ell}(x, y), \ \ell = 1, ..., k$ through

$$p_{\ell,\ell}(x, y) = \frac{1}{\gamma_{\ell,\ell}} q_\ell(x, y) - \frac{\gamma_{\ell-1,\ell}}{\gamma_{\ell,\ell}} p_{\ell-1,\ell}(x, y), \ \ell = 1, ..., k, \tag{3.4}$$

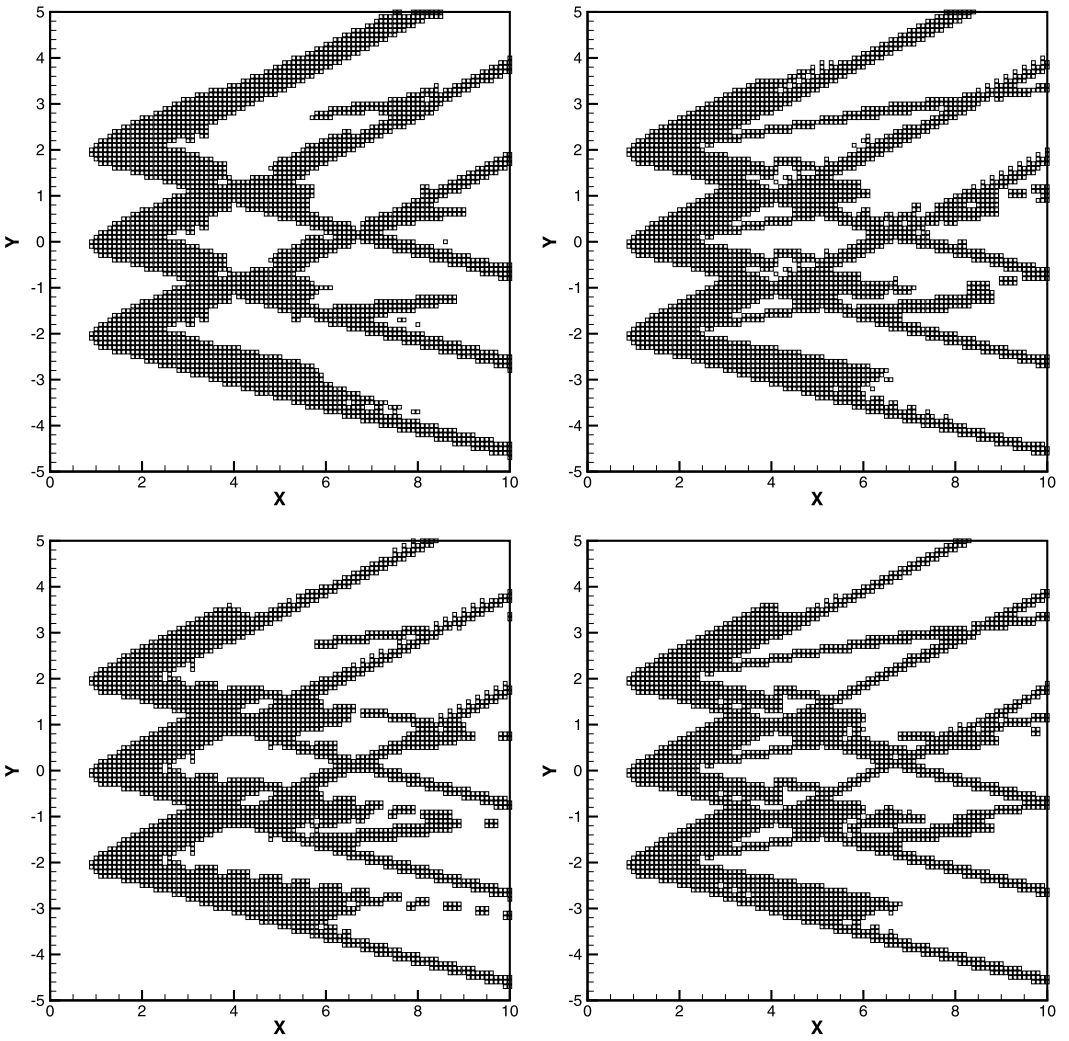

Fig. 7. A supersonic flow past three plates with an attack angle. Squares denote cells which are identified as troubled cells subject to multi-resolution WENO limiting procedures at the last time step. From left to right and top to bottom: second-order, third-order, fourth-order, and fifth-order methods. 100×100 cells.

with $\gamma_{\ell-1,\ell} + \gamma_{\ell,\ell} = 1$ and $\gamma_{\ell,\ell} \neq 0$, together with polynomials $p_{\ell,\ell+1}(x, y),\ \ell = 1, ..., k-1$ through

$$p_{\ell,\ell+1}(x, y) = \omega_{\ell,\ell} p_{\ell,\ell}(x, y) + \omega_{\ell-1,\ell} p_{\ell-1,\ell}(x, y),\ \ell = 1, ..., k-1, \tag{3.5}$$

with $\omega_{\ell-1,\ell} + \omega_{\ell,\ell} = 1$. In (3.4), the γ's are the linear weights and we choose them as $\gamma_{\ell-1,\ell} = 0.01$ and $\gamma_{\ell,\ell} = 0.99$ for the numerical computations of all steady-state problems. In (3.5), the ω's are the nonlinear weights which will be defined later. The smoothness indicators β_{ℓ,ℓ_2} are computed by using the same recipe as in [27]:

$$\beta_{\ell,\ell_2} = \sum_{|\alpha|=1}^{\kappa} \int_{I_{i,j}} \left(\Delta x_i \Delta y_j\right)^{|\alpha|-1} \left(\frac{\partial^{|\alpha|}}{\partial x^{\alpha_1} \partial y^{\alpha_2}} p_{\ell,\ell_2}(x, y)\right)^2 dx\, dy,\ \ell = \ell_2 - 1, \ell_2;\ \ell_2 = 1, ..., k, \tag{3.6}$$

where $\kappa = \ell$, $\alpha = (\alpha_1, \alpha_2)$, and $|\alpha| = \alpha_1 + \alpha_2$, respectively. The only exception is $\beta_{0,1}$, which is specified in [58]. We adopt the WENO-Z recipe as shown in [4,7] to compute the nonlinear weights [58]. Finally, the new reconstruction polynomial is defined as

$$u_h^{new}|_{I_{i,j}} = \sum_{\ell=\ell_2-1}^{\ell_2} \omega_{\ell,\ell_2} p_{\ell,\ell_2}(x, y),\ \ \ell_2 = 1, ..., k, \tag{3.7}$$

for obtaining (k+1)th-order spatial approximation. The two-dimensional system cases [58] are omitted here to save space.

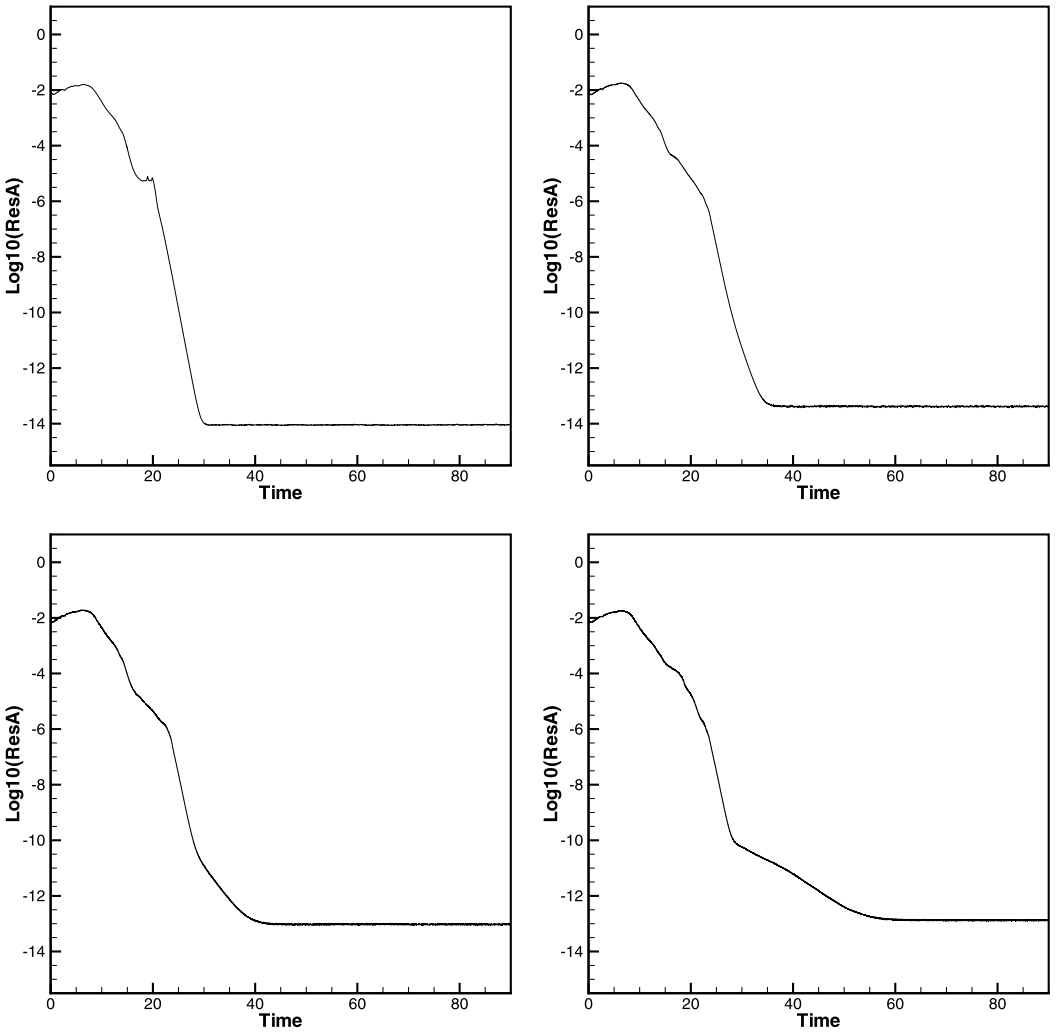

Fig. 8. A supersonic flow past three plates with an attack angle. The evolution of the average numerical residual of RKDG methods with multi-resolution WENO limiters. From left to right and top to bottom: second-order, third-order, fourth-order, and fifth-order methods. 100×100 cells.

Remarks. In this paper, we apply the new multi-resolution WENO schemes as limiters for high-order RKDG methods to compute steady-state problems. The crucial advantages of these multi-resolution WENO limiters are the compactness of their spatial stencils, which essentially only contain the troubled cell itself with information from intermediate neighboring four cells used only to determine the smoothness indicator of the zeroth degree polynomial in the hierarchy. In order to keep the advantages of the compact stencil, we use orthogonal basis and L^2 projection to define the sequence of hierarchical polynomials of different degrees in the troubled cell itself. This methodology facilitates the achievement of the conservation and the maintenance of as much information of the original polynomial in the troubled cell as possible through the mechanism of a gradual degradation to zeroth degree polynomial in a L^2 projection fashion with the spatial WENO procedure. Numerical experiments on benchmark steady-state problems specified in next section indicate the good behavior of the high-order RKDG methods with such multi-resolution WENO limiters.

4. Numerical tests

In this section, we perform numerical experiments to test the steady-state computation performance of high-order RKDG methods with multi-resolution WENO limiters described in the previous sections. The CFL number is 0.3 for the second-order (P^1), 0.18 for the third-order (P^2), 0.1 for the fourth-order (P^3), and 0.08 for the fifth-order (P^4) RKDG methods, respectively. For solving two-dimensional steady-state problems, the time step is chosen according to the CFL condition

$$\Delta t \max_{1\le i\le N}\left(\frac{|\mu_i|+c_i}{h_i}+\frac{|\nu_i|+c_i}{h_i}\right)\le CFL,$$

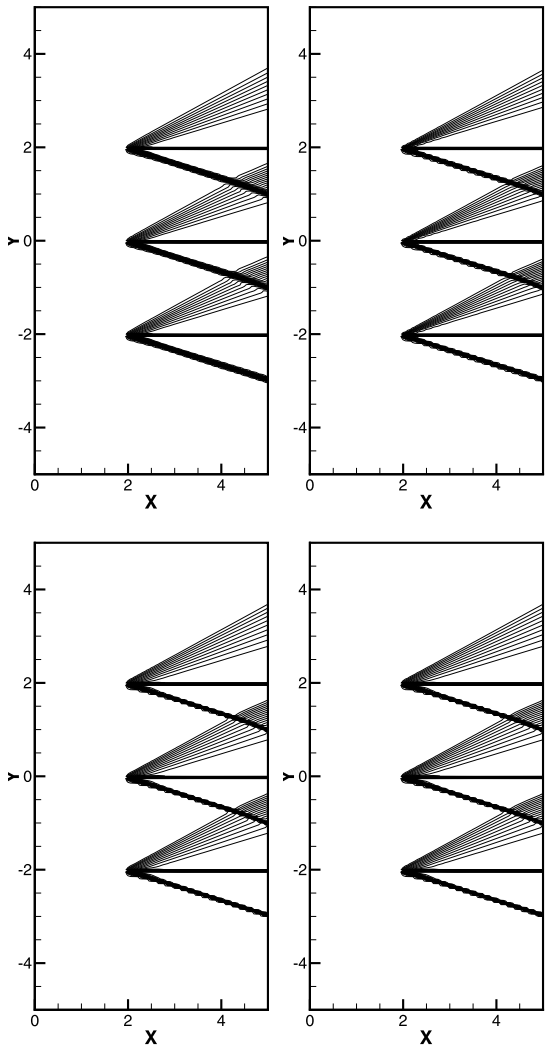

Fig. 9. A supersonic flow past three long plates problem. 30 equally spaced pressure contours from 0.031 to 0.161 of RKDG methods with multi-resolution WENO limiters. From left to right and top to bottom: second-order, third-order, fourth-order, and fifth-order methods. 100×200 cells.

in which μ_i is x-directional velocity, ν_i is y-directional velocity, $c_i = \sqrt{\frac{\gamma p_i}{\rho_i}}$, h_i is the diameter of the inscribed circle of the target cell, and N is the total number of the cells. The single index i is used here to list all cells in the computational field. Then the average numerical residual is defined as

$$Res_A = \sum_{i=1}^{N} \frac{|R1_i| + |R2_i| + |R3_i| + |R4_i|}{4 \times N}, \tag{4.1}$$

where $R*_i$ are the local numerical residuals of different cell averages of the conservative variables, that is, $R1_i = \frac{\partial \rho}{\partial t}|_i \approx \frac{\rho_i^{n+1} - \rho_i^n}{\Delta t}$, $R2_i = \frac{\partial (\rho\mu)}{\partial t}|_i \approx \frac{(\rho\mu)_i^{n+1} - (\rho\mu)_i^n}{\Delta t}$, $R3_i = \frac{\partial (\rho\nu)}{\partial t}|_i \approx \frac{(\rho\nu)_i^{n+1} - (\rho\nu)_i^n}{\Delta t}$, and $R4_i = \frac{\partial E}{\partial t}|_i \approx \frac{E_i^{n+1} - E_i^n}{\Delta t}$, respectively. All cells are set to be troubled cells in Example 4.1, so as to test numerical accuracy when the new type of multi-resolution WENO limiting procedure is enacted in the whole computational field. Then we set the constant C_k in (3.1) to be 1 in other steady-state problems.

Example 4.1. In this accuracy example, we study two-dimensional Euler equations

$$\frac{\partial}{\partial t}\begin{pmatrix} \rho \\ \rho\mu \\ \rho\nu \\ E \end{pmatrix} + \frac{\partial}{\partial x}\begin{pmatrix} \rho\mu \\ \rho\mu^2 + p \\ \rho\mu\nu \\ \mu(E+p) \end{pmatrix} + \frac{\partial}{\partial y}\begin{pmatrix} \rho\nu \\ \rho\mu\nu \\ \rho\nu^2 + p \\ \nu(E+p) \end{pmatrix} = 0, \tag{4.2}$$

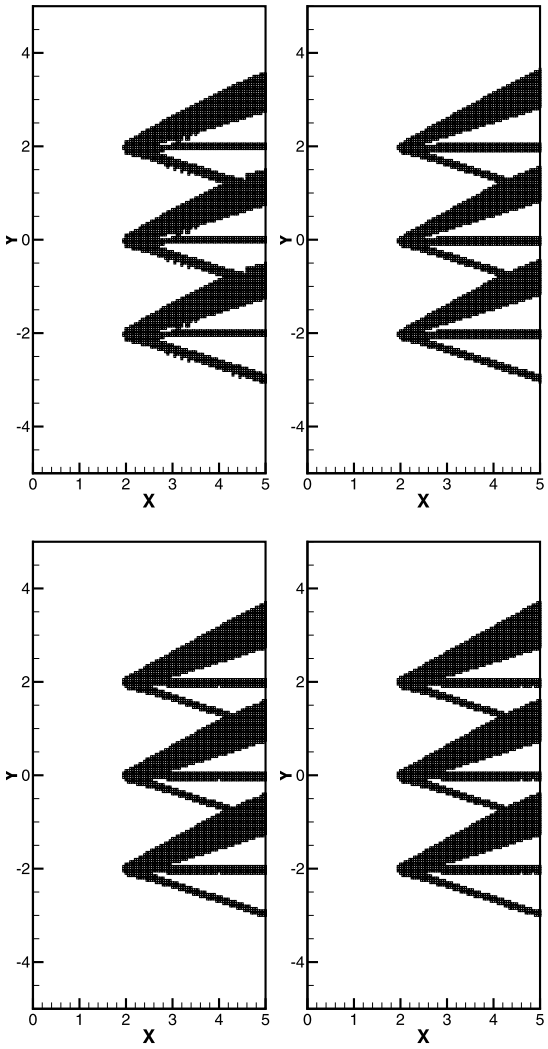

Fig. 10. A supersonic flow past three long plates problem. Squares denote cells which are identified as troubled cells subject to multi-resolution WENO limiting procedures at the last time step. From left to right and top to bottom: second-order, third-order, fourth-order, and fifth-order methods. 100×200 cells.

with the exact steady-state solutions given by (1) $\rho(x, y, \infty) = 1 + 0.2\sin(x - y)$, $\mu(x, y, \infty) = 1$, $\nu(x, y, \infty) = 1$, and $p(x, y, \infty) = 1$; (2) $\rho(x, y, \infty) = 1 + 0.2\sin(2(x - y))$, $\mu(x, y, \infty) = 1$, $\nu(x, y, \infty) = 1$, and $p(x, y, \infty) = 1$. We take the numerical initial conditions as the exact solution projected onto the grid, and then march to numerical steady states. The computational domain is $(x, y) \in [0, 2] \times [0, 2]$, and the exact steady-state solutions are applied as boundary conditions in both directions. The convergence history of the numerical residual (4.1) as a function of time is shown in Fig. 1 and Fig. 2, in which we can see that the numerical residual settles down to tiny numbers close to machine zero. The L^1 and L^∞ errors and orders of accuracy at steady state are listed in Table 1 and Table 2, from which we can see that the designed second-order, third-order, fourth-order, and fifth-order accuracies are achieved for RKDG methods with multi-resolution WENO limiters.

Example 4.2. Shock reflection problem. The computational domain is a rectangle of length 4 and height 1. The boundary conditions are that of a reflection condition along the bottom boundary, supersonic outflow along the right boundary, and Dirichlet conditions on the other two sides:

$$(\rho, \mu, \nu, p)^T) = \begin{cases} (1.0, 2.9, 0, 1.0/1.4)^T|_{(0,y,t)^T}, \\ (1.69997, 2.61934, -0.50632, 1.52819)^T|_{(x,1,t)^T}. \end{cases}$$

Initially, we set the solution in the entire domain to be that at the left boundary. We show the density contours with 15 equally spaced contour lines from 1.10 to 2.58 when steady states are reached for different orders of RKDG methods with multi-resolution WENO limiters in Fig. 3. The troubled cells identified at the final time step are shown in Fig. 4. We can clearly observe that the fifth-order RKDG method with the associated multi-resolution WENO limiter gives better resolution

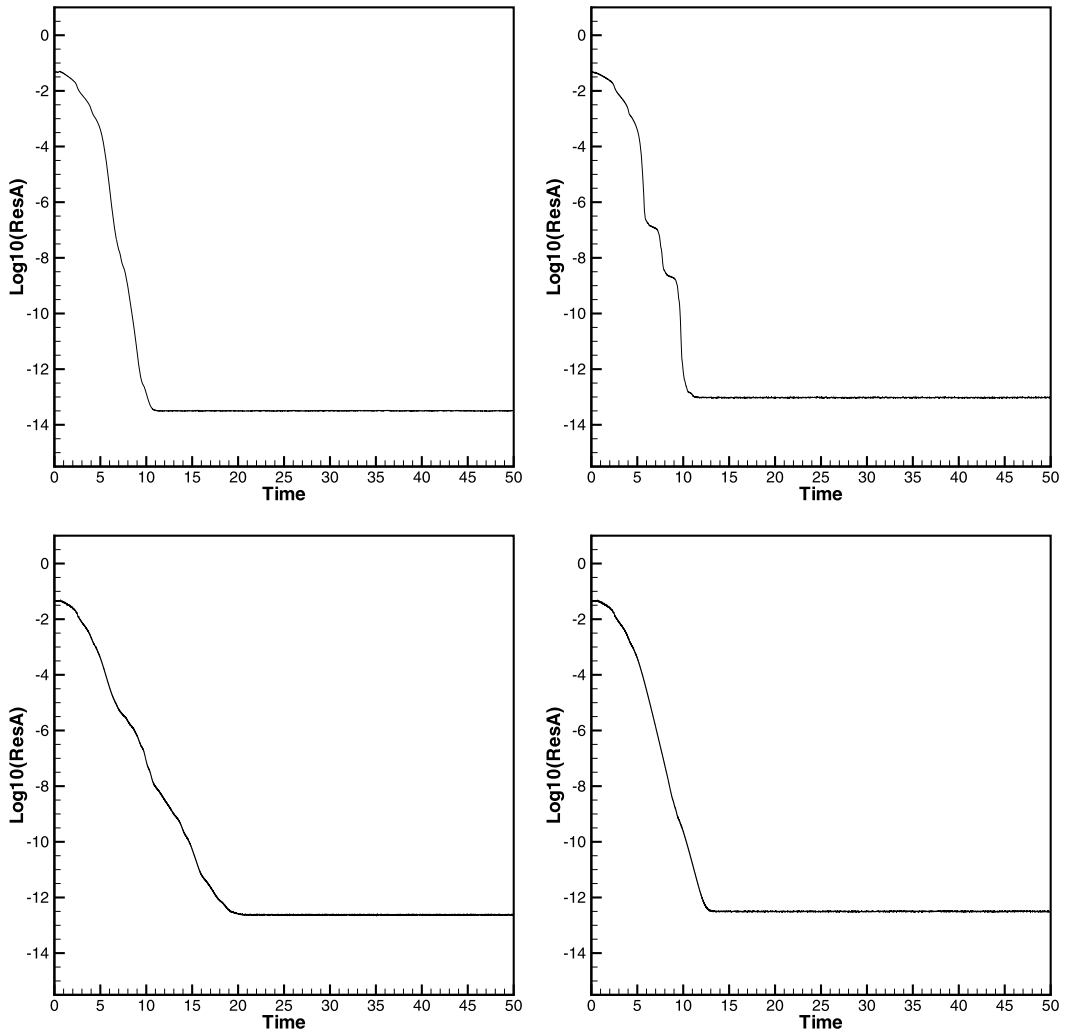

Fig. 11. A supersonic flow past three long plates problem. The evolution of the average numerical residual of RKDG methods with multi-resolution WENO limiters. From left to right and top to bottom: second-order, third-order, fourth-order, and fifth-order methods. 100×200 cells.

than that of the lower order RKDG methods, especially for obtaining sharp shock transitions. The convergence history of the numerical residual (4.1) as a function of time is shown in Fig. 5. It can be observed that the average residual of second-order, third-order, fourth-order, and fifth-order RKDG methods with multi-resolution WENO limiters can settle down to a value around $10^{-11.5}$, close to machine zero.

Example 4.3. This problem is a supersonic flow past three plates with an attack angle of $\alpha = 10^{\circ}$. The free stream Mach number is $M_{\infty} = 3$. The ideal gas goes from the left toward the plates. The initial conditions are set as $p = \frac{1}{\gamma M_{\infty}^2}$, $\rho = 1$, $\mu = \cos(\alpha)$, and $\nu = \sin(\alpha)$. The computational field is $[0, 10] \times [-5, 5]$. Three plates are set at $x \in [1, 2]$ with $y = -2$, $x \in [1, 2]$ with $y = 0$, and $x \in [1, 2]$ with $y = 2$. The slip boundary condition is imposed on three plates. The physical values of the inflow and outflow boundary conditions are applied in different directions. The results are shown when the numerical solutions reach their steady states. We show 30 equally spaced pressure contours from 0.02 to 0.24 computed by the different orders of RKDG methods with multi-resolution WENO limiters in Fig. 6. The troubled cells identified at the final time step are shown in Fig. 7. The convergence history of the numerical residual (4.1) is shown in Fig. 8. More noticeably, the average numerical residual of the second-order, third-order, fourth-order, and fifth-order RKDG methods with associated multi-resolution WENO limiters can settle down to a tiny value around 10^{-13}, close to machine zero. Although the boundary is very far away from the three plates, the shock waves, the rarefaction waves, and their interaction waves propagate to the far field boundaries. It often causes the numerical residual of high-order RKDG methods with WENO limiters from settling down to machine zero. But it does not seem to cause much trouble for the different orders of RKDG methods with multi-resolution WENO limiters specified in this paper.

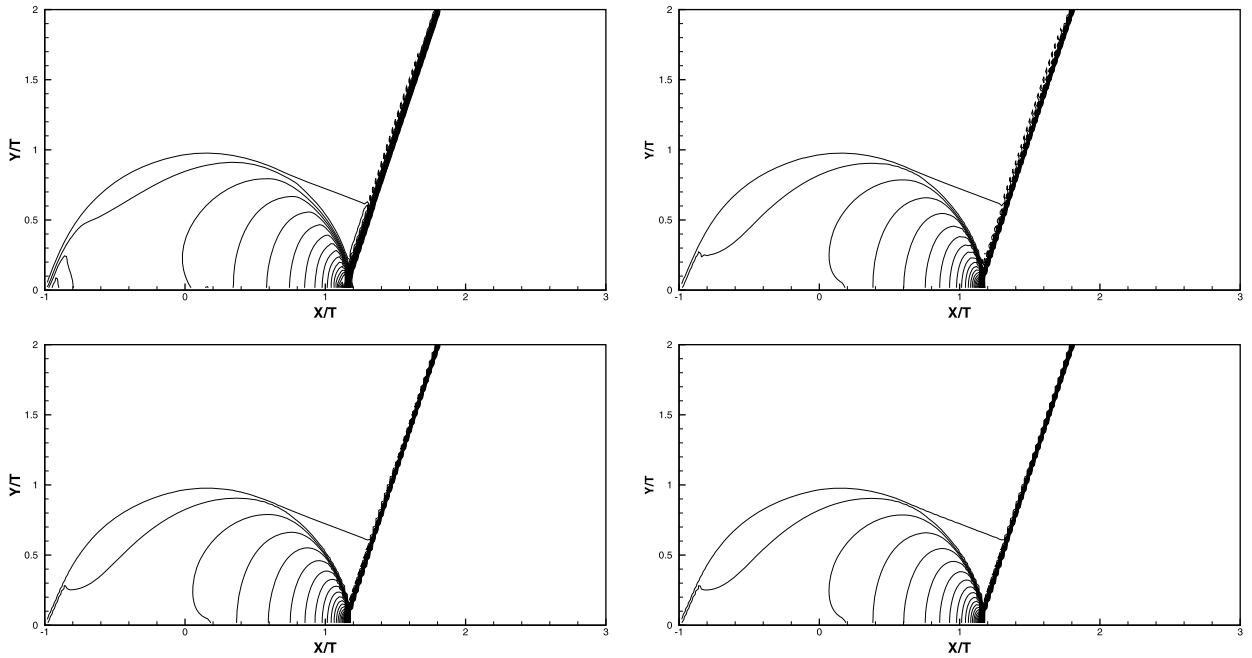

Fig. 12. The self-similar Mach reflection problem. 40 equally spaced pressure contours from 1.02 to 1.36 of RKDG methods with multi-resolution WENO limiters. From left to right and top to bottom: second-order, third-order, fourth-order, and fifth-order methods. 200×100 cells.

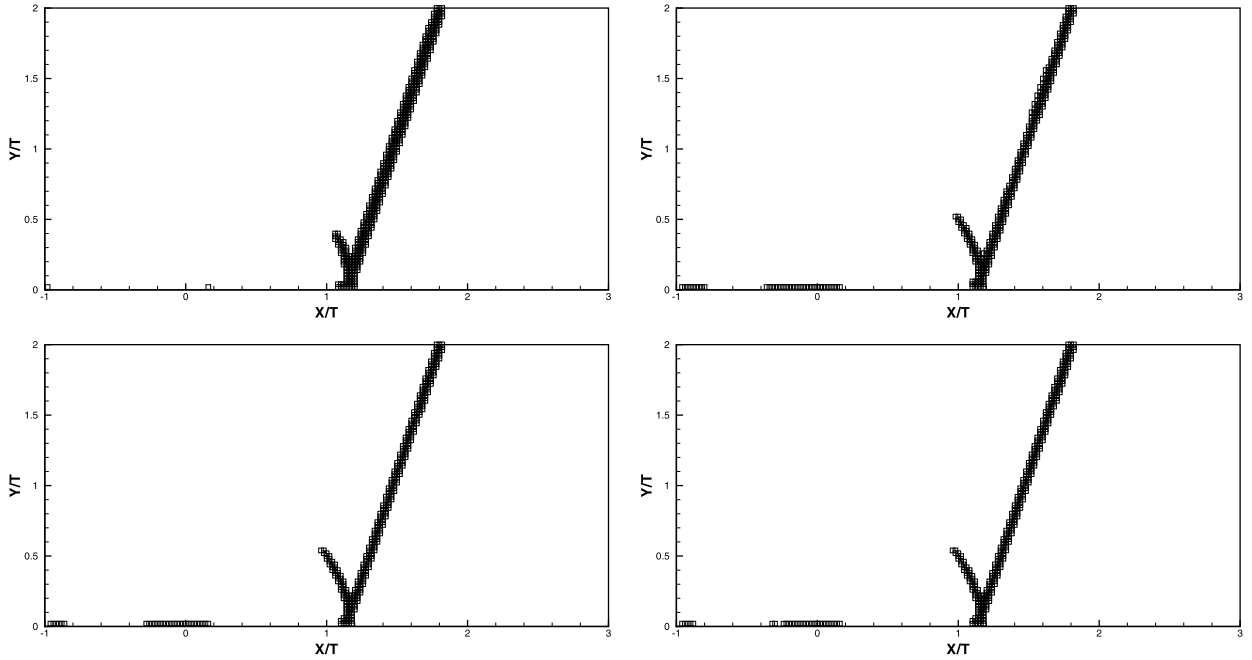

Fig. 13. The self-similar Mach reflection problem. Squares denote cells which are identified as troubled cells subject to multi-resolution WENO limiting procedures at the last time step. From left to right and top to bottom: second-order, third-order, fourth-order, and fifth-order methods. 200×100 cells.

Example 4.4. This problem is a supersonic flow past three long plates with an attack angle of $\alpha = 10^\circ$. The free stream Mach number is $M_\infty = 3$. The ideal gas goes from the left toward three long plates. The initial condition is set as $p = \frac{1}{\gamma M_\infty^2}$, $\rho = 1$, $\mu = \cos(\alpha)$, and $\nu = \sin(\alpha)$. The computational field is $[0, 5] \times [-5, 5]$. Three long plates are set at $x \in [2, 5]$ with $y = -2$, $x \in [2, 5]$ with $y = 0$, and $x \in [2, 5]$ with $y = 2$. The slip boundary condition is imposed on three long plates. The physical values of the inflow and outflow boundary conditions are applied at the left, right, bottom, and top boundaries. The results are shown when the numerical solutions have settled down to their steady states. We show 30 equally spaced pressure contours from 0.031 to 0.161 computed by the different orders of RKDG methods with multi-resolution WENO

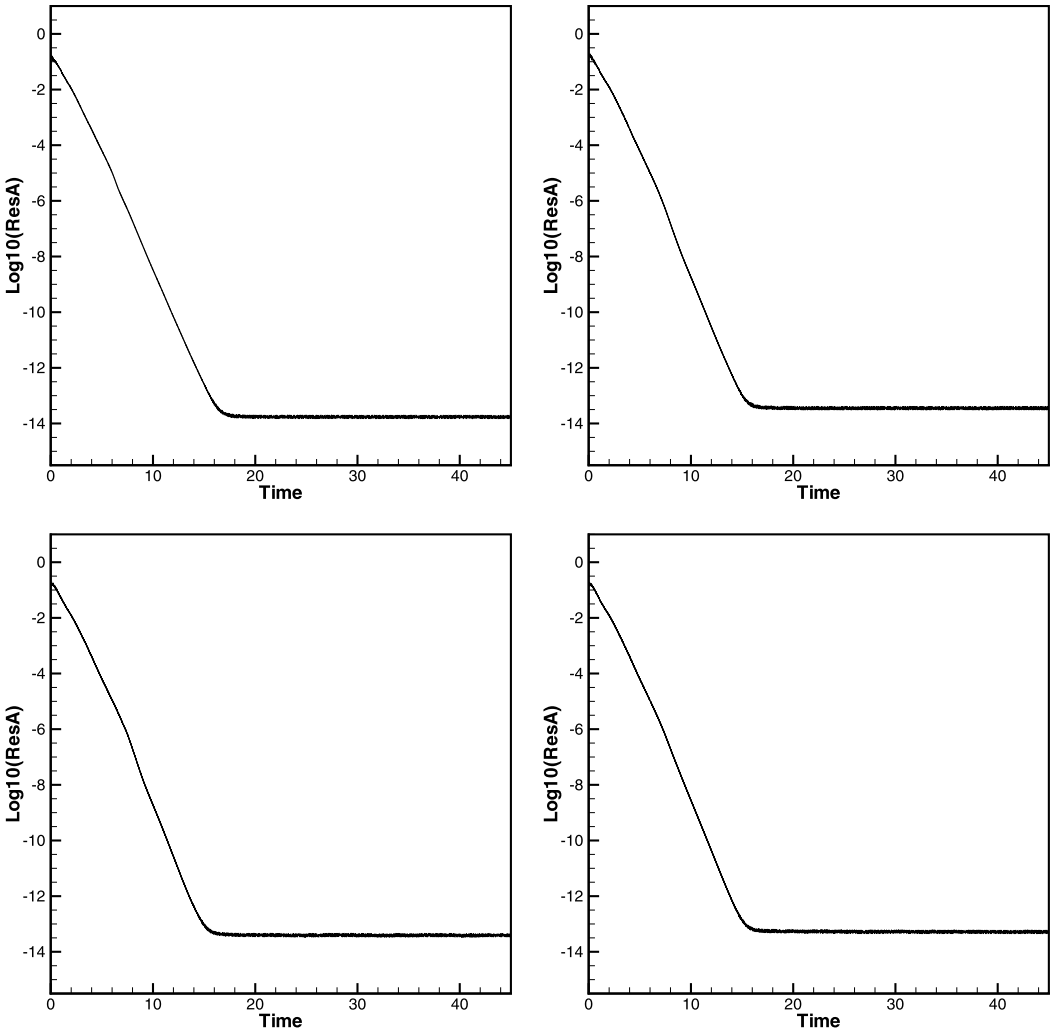

Fig. 14. The self-similar Mach reflection problem. The evolution of the average numerical residual of RKDG methods with multi-resolution WENO limiters. From left to right and top to bottom: second-order, third-order, fourth-order, and fifth-order methods. 200×100 cells.

limiters in Fig. 9. The troubled cells identified at the final time step are shown in Fig. 10. The convergence history of the numerical residual (4.1) is shown in Fig. 11. We can find that the average numerical residual of high-order RKDG methods with multi-resolution WENO limiters settles down to a value around $10^{-12.5}$, close to machine zero. In this case, the shocks, the rarefaction waves, and their interactions all pass through the right boundary. It is one of the reasons that numerical residuals for many high-order schemes such as other high-order RKDG methods with WENO/HWENO limiters do not converge to machine zero, however this does not seem to be the case for the RKDG methods with multi-resolution WENO limiters in this paper.

Example 4.5. We compute the numerical solution of (4.2) with $U(x, y, t) = (\rho, \mu, \nu, p)^T$, in which $U(x, y, 0) = \begin{cases} U_R \equiv (\rho_R, 0, 0, p_R)^T, & \text{if } x > 0, \\ U_L \equiv (\rho_L, \mu_L, 0, p_L)^T, & \text{if } x < 0, \end{cases}$ where the left-hand and right-hand states are connected by the Rankine-Hugoniot jump conditions for a shock with Mach number M. The boundary condition on the wedge wall is $(\mu, \nu) \cdot \vec{n} = 0$ and $\vec{n}$ is the unit normal vector at the wall for a shock Mach number equal to 1.075 and a wedge angle θ equal to 15 degrees in [49]. These data correspond to the parameter $a \approx \frac{1}{2}$ in the UTSDE model specified in [48]. This problem is well outside the range for which regular reflection can occur. However, Mach reflection is also not possible for shocks this weak, and so this example illustrates a classic triple point paradox. Since this problem is self-similar, the solution depends on the similarity variables $\xi = \frac{x}{t}$ and $\eta = \frac{y}{t}$, respectively. We rewrite (4.2) as $U_t + F_x + G_y = 0$, where $U = (\rho, \rho\mu, \rho\nu, E)^T$, $F = (\rho\mu, \rho\mu^2 + p, \rho\mu\nu, \mu(E + p))^T$, and $G = (\rho\nu, \rho\mu\nu, \rho\nu^2 + p, \nu(E + p))^T$. Then we write it in terms of ξ, η, and a pseudo time variable $\tau = \log t$. We can obtain $U_\tau + (F - \xi U)_\xi + (G - \eta U)_\eta + 2U = 0$. In these self-similar variables, the Euler system has the form of the unsteady equations (4.2) with modified flux functions and a source term. On the condition

that $\tau \to +\infty$, the solution of $U_\tau + (F - \xi U)_\xi + (G - \eta U)_\eta + 2U = 0$ converges to a pseudo steady, self-similar solution that satisfies $(F - \xi U)_\xi + (G - \eta U)_\eta + 2U = 0$. In our computations, we rotate the original computational domain specified in [49] with a angle θ equal to 15 degrees, and set the new computational domain as $(\xi, \eta) \in [-1, 3] \times [0, 2]$, use $\rho_R = 1.4$ and $p_R = 1$, and determine the values U_L behind the shock from the Rankine-Hugoniot conditions. The reflection boundary condition is used at the wall, which for the rest of the bottom boundary (the part from $\xi = -1$ to $\xi = \frac{1}{6}$), the exact post-shock condition is imposed. At the top boundary is the exact motion of the Mach 1.075 shock. The results are shown when the numerical solutions have settled down to their steady states. We show 40 equally spaced pressure contours from 1.02 to 1.36 computed by the different orders of RKDG methods with multi-resolution WENO limiters in Fig. 12. The troubled cells identified at the final time step are shown in Fig. 13. The convergence history of the numerical residual (4.1) is shown in Fig. 14. We can find that the average numerical residual of high-order RKDG methods with multi-resolution WENO limiters settles down to a value around $10^{-13.5}$, close to machine zero.

5. Concluding remarks

In this paper, we design a new troubled cell indicator and adopt our high-order finite volume multi-resolution WENO schemes [59] to serve as limiters for high-order RKDG methods to solve two-dimensional steady-state problems on structured meshes. The general framework of such multi-resolution WENO limiters for high-order RKDG methods is to first design a new methodology to detect troubled cells subject to the multi-resolution WENO limiting procedure, then to construct a sequence of hierarchical L^2 projection polynomial solutions of the DG methods completely restricted to the troubled cell itself in a WENO fashion. To the best of our knowledge, it is the first time that numerical residual for second-order, third-order, fourth-order, and fifth-order RKDG methods with multi-resolution WENO limiters can settle down close to machine zero for benchmark steady-state problems, including some problems containing strong shocks, contact discontinuities, rarefaction waves, their interactions, and associated compound sophisticated waves passing through boundaries. The results in this paper indicate that these new high-order RKDG methods with multi-resolution WENO limiters have a good potential in computing the steady-state problems, than other WENO type limiters for the RKDG methods together with some classical troubled cell indicators [8–12,28,42,43,58].

The framework of this new type of multi-resolution WENO limiters for arbitrary high-order RKDG methods would be particularly efficient and simple for solving steady-state problems on unstructured meshes (such as triangular meshes or tetrahedral meshes), and the study of which is our ongoing work.

References

[1] D. Balsara, C. Altmann, C. Munz, M. Dumbser, A sub-cell based indicator for troubled zones in RKDG schemes and a novel class of hybrid RKDG+HWENO schemes, J. Comput. Phys. 226 (2007) 586–620.
[2] T.J. Barth, D. Jespersen, The design and application of upwind schemes on unstructured meshes, in: AIAA Paper, 89-0366, 1989.
[3] R. Biswas, K.D. Devine, J. Flaherty, Parallel, adaptive finite element methods for conservation laws, Appl. Numer. Math. 14 (1994) 255–283.
[4] R. Borges, M. Carmona, B. Costa, W.S. Don, An improved weighted essentially non-oscillatory scheme for hyperbolic conservation laws, J. Comput. Phys. 227 (2008) 3191–3211.
[5] A. Burbeau, P. Sagaut, C.H. Bruneau, A problem-independent limiter for high-order Runge-Kutta discontinuous Galerkin methods, J. Comput. Phys. 169 (2001) 111–150.
[6] G. Capdeville, A central WENO scheme for solving hyperbolic conservation laws on non-uniform meshes, J. Comput. Phys. 227 (2008) 2977–3014.
[7] M. Castro, B. Costa, W.S. Don, High order weighted essentially non-oscillatory WENO-Z schemes for hyperbolic conservation laws, J. Comput. Phys. 230 (2011) 1766–1792.
[8] B. Cockburn, S. Hou, C.-W. Shu, The Runge-Kutta local projection discontinuous Galerkin finite element method for conservation laws IV: the multidimensional case, Math. Comput. 54 (1990) 545–581.
[9] B. Cockburn, S.-Y. Lin, C.-W. Shu, TVB Runge-Kutta local projection discontinuous Galerkin finite element method for conservation laws III: one dimensional systems, J. Comput. Phys. 84 (1989) 90–113.
[10] B. Cockburn, C.-W. Shu, TVB Runge-Kutta local projection discontinuous Galerkin finite element method for conservation laws II: general framework, Math. Comput. 52 (1989) 411–435.
[11] B. Cockburn, C.-W. Shu, The Runge-Kutta local projection P1-discontinuous Galerkin finite element method for scalar conservation laws, Modél. Math. Anal. Numér. 25 (1991) 337–361.
[12] B. Cockburn, C.-W. Shu, The Runge-Kutta discontinuous Galerkin method for conservation laws V: multidimensional systems, J. Comput. Phys. 141 (1998) 199–224.
[13] B. Cockburn, C.-W. Shu, Runge-Kutta discontinuous Galerkin method for convection-dominated problems, J. Sci. Comput. 16 (2001) 173–261.
[14] M. Dumbser, Arbitrary High Order Schemes for the Solution of Hyperbolic Conservation Laws in Complex Domains, Shaker Verlag, Aachen, 2005.
[15] M. Dumbser, Arbitrary high order P.N.M schemes on unstructured meshes for the compressible Navier-Stokes equations, Comput. Fluids 39 (2010) 60–76.
[16] M. Dumbser, D.S. Balsara, E.F. Toro, C.D. Munz, A unified framework for the construction of one-step finite volume and discontinuous Galerkin schemes on unstructured meshes, J. Comput. Phys. 227 (2008) 8209–8253.
[17] M. Dumbser, O. Zanotti, R. Loubere, S. Diot, A posteriori subcell limiting of the discontinuous Galerkin finite element method for hyperbolic conservation laws, J. Comput. Phys. 278 (2014) 47–75.
[18] O. Friedrichs, Weighted essentially non-oscillatory schemes for the interpolation of mean values on unstructured grids, J. Comput. Phys. 144 (1998) 194–212.
[19] G. Fu, C.-W. Shu, A new troubled-cell indicator for discontinuous Galerkin methods for hyperbolic conservation laws, J. Comput. Phys. 347 (2017) 305–327.
[20] A. Harten, High resolution schemes for hyperbolic conservation laws, J. Comput. Phys. 49 (1983) 357–393.
[21] X.J. He, D.H. Yang, X. Ma, A weighted Runge-Kutta discontinuous Galerkin method for 3D acoustic and elastic wave-field modeling, Commun. Comput. Phys. 28 (2020) 372–400.

[22] C. Hu, C.-W. Shu, Weighted essentially non-oscillatory schemes on triangular meshes, J. Comput. Phys. 150 (1999) 97–127.
[23] A. Jameson, Steady state solutions of the Euler equations for transonic flow by a multigrid method, in: Advances in Scientific Computing, Academic Press, 1982, pp. 37–70.
[24] A. Jameson, Artificial diffusion, upwind biasing, limiters and their effect on accuracy and multigrid convergence in transonic and hypersonic flows, in: AIAA Paper, 93-3359, 1993.
[25] A. Jameson, A perspective on computational algorithms for aerodynamic analysis and design, Prog. Aerosp. Sci. 37 (2001) 197–243.
[26] A. Jameson, W. Schmidt, E. Turkel, Numerical solution of the Euler equations by finite volume methods using Runge-Kutta time-stepping schemes, in: AIAA Paper, 1981-1259, 1981.
[27] G. Jiang, C.-W. Shu, Efficient implementation of weighted ENO schemes, J. Comput. Phys. 126 (1996) 202–228.
[28] L. Krivodonova, J. Xin, J.-F. Remacle, N. Chevaugeon, J.E. Flaherty, Shock detection and limiting with discontinuous Galerkin methods for hyperbolic conservation laws, Appl. Numer. Math. 48 (2004) 323–338.
[29] B. van Leer, S. Nomura, Discontinuous Galerkin for diffusion, in: Proceedings of 17th AIAA Computational Fluid Dynamics Conference, June 6–9, 2005, AIAA-2005-5108.
[30] D. Levy, G. Puppo, G. Russo, Central WENO schemes for hyperbolic systems of conservation laws, M2AN. Math. Model. Numer. Anal. 33 (1999) 547–571.
[31] D. Levy, G. Puppo, G. Russo, Compact central WENO schemes for multidimensional conservation laws, SIAM J. Sci. Comput. 22 (2000) 656–672.
[32] X. Liu, S. Osher, T. Chan, Weighted essentially non-oscillatory schemes, J. Comput. Phys. 115 (1994) 200–212.
[33] J.L. Lou, L. Li, H. Luo, H. Nishikawa, Reconstructed discontinuous Galerkin methods for linear advection-diffusion equations based on first-order hyperbolic system, J. Comput. Phys. 369 (2018) 103–124.
[34] H. Luo, J.D. Baum, R. Lohner, A Hermite WENO-based limiter for discontinuous Galerkin method on unstructured grids, J. Comput. Phys. 225 (2007) 686–713.
[35] H. Luo, J.D. Baum, R. Lohner, A discontinuous Galerkin method based on a Taylor basis for the compressible flows on arbitrary grids, J. Comput. Phys. 227 (2008) 8875–8893.
[36] H. Luo, L. Luo, R. Nourgaliev, V.A. Mousseau, N. Dinh, A reconstructed discontinuous Galerkin method for the compressible Navier-Stokes equations on arbitrary grids, J. Comput. Phys. 229 (2010) 6961–6978.
[37] H. Luo, Y. Xia, S. Li, R. Nourgaliev, C. Cai, A Hermite WENO reconstruction-based discontinuous Galerkin method for the equations on tetrahedral grids, J. Comput. Phys. 231 (2012) 5489–5503.
[38] H. Luo, H. Xiao, R. Nourgaliev, C. Cai, A comparative study of different reconstruction schemes for a reconstructed discontinuous Galerkin method on arbitrary grids, in: Proceedings of AIAA, 11-3839, 2011.
[39] H. Luo, Y. Xia, S. Spiegel, R. Nourgaliev, Z. Jiang, A reconstructed discontinuous Galerkin method based on a hierarchical WENO reconstruction for compressible flows on tetrahedral grids, J. Comput. Phys. 236 (2013) 477–492.
[40] R.D. Nair, M.N. Levy, P.H. Lauritzen, Emerging numerical methods for atmospheric modeling, in: P.H. Lauritzen, C. Jablonowski, M.A. Taylor, R.D. Nair (Eds.), Numerical Techniques for Global Atmospheric Models, in: LNCSE, vol. 80, Springer-Verlag, 2011, pp. 189–250.
[41] S. Osher, C. Chakravarthy, High-resolution schemes and the entropy condition, SIAM J. Numer. Anal. 21 (1984) 955–984.
[42] J. Qiu, C.-W. Shu, Hermite WENO schemes and their application as limiters for Runge-Kutta discontinuous Galerkin method: one dimensional case, J. Comput. Phys. 193 (2003) 115–135.
[43] J. Qiu, C.-W. Shu, Runge-Kutta discontinuous Galerkin method using WENO limiters, SIAM J. Sci. Comput. 26 (2005) 907–929.
[44] W.H. Reed, T.R. Hill, Triangular mesh methods for neutron transport equation, Tech. Report LA-UR-73-479, Los Alamos Scientific Laboratory, 1973.
[45] S. Serna, A. Marquina, Power ENO methods: a fifth-order accurate weighted power ENO method, J. Comput. Phys. 194 (2004) 632–658.
[46] C.-W. Shu, Essentially non-oscillatory and weighted essentially non-oscillatory schemes for hyperbolic conservation laws, in: B. Cockburn, C. Johnson, C.-W. Shu, E. Tadmor, A. Quarteroni (Eds.), Advanced Numerical Approximation of Nonlinear Hyperbolic Equations, in: Lecture Notes in Mathematics, vol. 1697, Springer, Berlin, 1998, pp. 325–432.
[47] C.-W. Shu, S. Osher, Efficient implementation of essentially non-oscillatory shock-capturing schemes, J. Comput. Phys. 77 (1988) 439–471.
[48] A.M. Tesdall, J.K. Hunter, Self-similar solutions for weak shock reflection, SIAM J. Appl. Math. 63 (2002) 42–61.
[49] A.M. Tesdall, R. Sanders, B.L. Keyfitz, Self-similar solutions for the triple point paradox in gasdynamics, SIAM J. Appl. Math. 68 (2008) 1360–1377.
[50] V. Venkatakrishnan, Convergence to steady state solutions of the Euler equations on unstructured grids with limiters, J. Comput. Phys. 118 (1995) 120–130.
[51] L. Wu, Y.-T. Zhang, S. Zhang, C.-W. Shu, High order fixed-point sweeping WENO methods for steady state of hyperbolic conservation laws and its convergence study, Commun. Comput. Phys. 20 (2016) 835–869.
[52] H.C. Yee, A. Harten, Implicit TVD schemes for hyperbolic conservation laws in curvilinear coordinates, AIAA J. 25 (1987) 266–274.
[53] H.C. Yee, R.F. Warming, A. Harten, Implicit total variation diminishing (TVD) schemes for steady-state calculations, J. Comput. Phys. 57 (1985) 327–360.
[54] S. Zhang, S. Jiang, C.-W. Shu, Improvement of convergence to steady state solutions of Euler equations with the WENO schemes, J. Sci. Comput. 47 (2011) 216–238.
[55] L. Zhang, W. Liu, L. He, X. Deng, H. Zhang, A class of hybrid DG/FV methods for conservation laws I: basic formulation and one-dimensional systems, J. Comput. Phys. 231 (2012) 1081–1103.
[56] L. Zhang, W. Liu, L. He, X. Deng, H. Zhang, A class of hybrid DG/FV methods for conservation laws II: two-dimensional cases, J. Comput. Phys. 231 (2012) 1104–1120.
[57] S. Zhang, C.-W. Shu, A new smoothness indicator for WENO schemes and its effect on the convergence to steady state solutions, J. Sci. Comput. 31 (2007) 273–305.
[58] J. Zhu, J. Qiu, C.-W. Shu, High-order Runge-Kutta discontinuous Galerkin methods with a new type of multi-resolution WENO limiters, J. Comput. Phys. 404 (2020) 109105.
[59] J. Zhu, C.-W. Shu, A new type of multi-resolution WENO schemes with increasingly higher order of accuracy, J. Comput. Phys. 375 (2018) 659–683.
[60] J. Zhu, C.-W. Shu, Convergence to steady-state solutions of the new type of high-order multi-resolution WENO schemes: a numerical study, Commun. Appl. Math. Comput. 2 (2020) 429–460.